The Egyptian Journal of Remote Sensing and Space Sciences 27 (2024) 108–119

Contents lists available at ScienceDirect

The Egyptian Journal of Remote Sensing and Space Sciences

journal homepage: www.sciencedirect.com

Research Paper

Automatic error correction: Improving annotation quality for model optimization in oil-exploration related land disturbances mapping

Yuwei Cai [a,b,1], Bingxu Hu [b,1], Hongjie He [b], Kyle Gao [c], Hongzhang Xu [b], Ying Zhang [d], Saied Pirasteh [a,e,*], Xiuqing Wang [a,*], Wenping Chen [a,*], Huxiong Li [a,*]

[a] Institute of Artificial Intelligence and School of Mechanical and Electrical Engineering, Shaoxing University, Shaoxing, ZJ 312000, China
[b] Department of Geography and Environmental Management, University of Waterloo, Waterloo, Ontario N2L 3G1, Canada
[c] Department Systems Design Engineering, University of Waterloo, Waterloo, Ontario N2L 3G1, Canada
[d] Canada Centre for Remote Sensing, Natural Resources Canada, Ottawa, Ontario K1S 5H4, Canada
[e] Department of Geotechnics and GeomaticsSaveetha School of Engineering Saveetha Institute of Medical and Technical Sciences, Chennai, Tamil Nadu, 602105, India

ARTICLE INFO

Keywords:
Deep-learning
Object-extraction
Land disturbance
Segmentation
Automatic error correction

ABSTRACT

The manual extraction of land disturbances associated with oil exploration, which normally includes resource roads, mining facilities, and well pads, presents significant challenges in terms of cost and time. Accurate monitoring and mapping of land disturbances resulting from oil exploration plays a crucial role in conducting comprehensive environmental assessments and facilitating effective land reclamation initiatives. However, prevailing deep learning methodologies in the realm of oil and gas exploration primarily focus on oil spill detection, neglecting the critical aspect of land disturbances resulting from oil exploration, thus overlooking the impact on land. Furthermore, given that the well sites are scattered and relatively diminutive compared to other land covers, their detection poses substantial difficulties. This paper proposes an automatic error-correcting (AEC) algorithm to address deficiencies in ground truth data quality. This AEC method was integrated into the deep-learning framework for land disturbance extraction, specifically tailored for land disturbances analysis associated with oil exploration. The efficacy of our method was validated on a dataset collected in Alberta covering an area of oil sand mining sites. The application of the AEC algorithm significantly enhanced the accuracy of land disturbance analysis, thereby contributing to a more effective hydrocarbon exploration impact analysis and facilitating the timely planning by the Alberta government. The results demonstrate notable improvements in both average pixel accuracy (AA) and mean intersection over union (mIoU), ranging from 8.3% to 15.4% and 0.5% to 5.8%, respectively. These enhancements, which have profound implications for the precision of land disturbance detection, prove that the proposed AEC algorithm can serve a dual purpose: correcting errors in the dataset and efficiently detecting land disturbance features in the oil exploration area.

1. Introduction

Precise and up-to-date maps of mining development footprints are crucial data for diverse planning endeavors in both urban and rural areas, including region conservation, emergency response, and land cover restoration (Safari et al., 2011; Liu et al., 2022; Li et al., 2022; Chen et al., 2022; Khorrami et al., 2023; Fu et al., 2023; Habibi et al., 2023). This research focuses specifically on Northern Alberta's oil sands mining region, a dynamic landscape with different backgrounds and extensive land disturbances resulting from oil and gas exploration activities. As oil infrastructure develops and transportation increases, the transition of forest or grassland areas into bare ground due to oil exploration poses a challenge in tracking, monitoring, and mapping. This transition is what we define as oil-exploration-related land disturbances. The dynamic nature of oil exploration operations adds complexity, making it a formidable challenge to accurately assess the environmental impacts and ensure effective reclamation (Laurence and Balmford, 2013; Kosari et al., 2020; Abdelfatah, 2023). Oil and gas

* Corresponding authors.
E-mail addresses: y99cai@uwaterloo.ca (Y. Cai), bingxu.hu@uwaterloo.ca (B. Hu), h69he@uwaterloo.ca (H. He), y56gao@uwaterloo.ca (K. Gao), h389xu@uwaterloo.ca (H. Xu), ying.zhang@NRCan-RNCan.gc.ca (Y. Zhang), sapirasteh1@usx.edu.cn (S. Pirasteh), wxq@usx.edu.cn (X. Wang), cwp@usx.edu.cn (W. Chen), spirasteh71@gmail.com, 2019000060@usx.edu.cn (H. Li).
[1] Co-first authors with equal contribution.

https://doi.org/10.1016/j.ejrs.2024.01.001
Received 26 October 2023; Received in revised form 8 January 2024; Accepted 17 January 2024
Available online 4 February 2024

exploration-related lands undergo changes through development, abandonment, or reclamation, and mapping these disturbances over vast areas, especially considering their rapid evolution, remains a significant challenge (Jordaan et al., 2009; Rokosh et al., 2012; Laurence and Balmford, 2013; Zhang et al., 2017; Thiessen and Achari, 2022). Despite the dispersed and comparatively diminutive nature of well sites established for oil exploration compared to other land covers, the cumulative alterations resulting from these scattered land disturbances can be substantial (Kearney et al., 2020; Hu, 2021). Contemporary research endeavors frequently emphasize oil spill detection, such as wind field corrections when oil spills (Li et al., 2022). However, there is a noticeable gap in the current research landscape, wherein the precise mapping of land disturbances attributable to oil exploration activities is inadequately addressed. This aspect assumes paramount importance in achieving a comprehensive environmental evaluation of oil exploration impacts. Despite the vital importance of comprehending the effects stemming from land disturbance associated with oil exploration, research endeavors in this domain have been notably constrained. In-situ oil/gas mining activities, which usually appear as small footprints in resource roads and well sites, are easily ignored or mistakenly detected. Therefore, it is crucial to procure accurate maps that detail the footprint extraction of land disturbances resulting from oil exploration.

This research uses deep learning (DL) methods and high-resolution satellite imagery to address these challenges for accurate land disturbance detection. Convolutional neural networks (CNNs)-based networks have demonstrated state-of-the-art results in relevant detection tasks (Maggiori et al., 2016; Ševo and Avramović, 2016; He et al., 2016; Máttyus et al., 2017; Sun et al., 2017; Volpi and Tuia, 2017; Chen et al., 2018; Dimitrovski et al., 2023). DL and CNN models are effective as they can rely significantly on the data quality used for training and testing, particularly when it comes to tasks like detecting land disturbances. Therefore, ensuring the accuracy of the examples can elevate the performance during image processing. However, if the examples contain errors, CNNs can learn to make incorrect generalizations and erroneous predictions (Simonyan and Zisserman, 2014; Yeh et al., 2020; Yekeen et al., 2020; Ma et al., 2021). To enhance model performance, an automatic error-correcting (AEC) algorithm is introduced in this study. The algorithm aims to improve the accuracy of the training dataset by rectifying potential errors, thereby enhancing the model's ability to generalize effectively when mapping labelled datasets.

In particular, we acknowledge that prior methodologies, such as FastICA (Sharifi and Amini, 2015; Sharifi et al., 2015), multivariate relevance vector regression (MVRVR) (Sharifi et al., 2016), relevance vector machine (RVM) (Sharifi, 2020), and multi-scale dual-branch residual spectral-spatial network (MDBRSSN) (Sharifi, 2021; Ghaderizadeh et al., 2022; Tariq et al., 2022; Farmonov et al., 2023), used on accurate mapping in rural or forested regions, experience significant challenge in improving performance when the detected target is small scale or when the dataset's quality is limited. Despite ongoing improvements in OpenStreetMap and crowdsource mapping efforts for paved roads, there remains a lack of accurate maps for unpaved service roads located in rural or forested regions. This gap in the available data can pose significant challenges for navigation and logistics planning (Shao et al., 2021). One of the particularly challenging tasks is mapping land disturbances, including service roads, well sites, and well pads, during and after oil exploration. Manually labelling roads and well pads is a process susceptible to errors, characterized by time consuming procedures, and often entails considerable expenses (Yang et al., 2018). For example, the detection of roads and well pads in rural areas is susceptible to errors and subjectivity (Fig. 1) due to the absence of regular mapping (Chowdhury et al., 2021). Furthermore, the ongoing expansion of resource road networks and well pads poses a challenge for detection tasks due to rapid infrastructure development. However, small-scale resource road networks and well pads have proven challenging to detect accurately in land disturbance mapping, leading to erroneous government monitoring and management (Laurence and Balmford, 2013). Through the identification and rectification of potential errors within the training examples, the AEC algorithm improves the model's capability to generalize effectively when mapping labelled datasets. Through this novel approach, our research contributes to the ongoing efforts in land disturbance detection and provides a clear perspective on the specific problems we aim to solve as compared to existing methods.

Moreover, we employed the imagery sourced from the state-of-the-art RapidEye satellite system. Renowned for its exceptional high-resolution capabilities, this satellite delivers a detailed perspective of the Alberta oil sands mining sites. The 500 × 500 pixel patches provide a finely detailed view of the terrain, enabling a nuanced comprehension of the features present. Within the dataset, a meticulous categorization has been executed, specifically focusing on identifying the presence of unpaved roads and well pads. These crucial components of the oil sands infrastructure are distinctly outlined within the images, adding a layer of specificity to the dataset. Notably, the dataset utilized in the research is annotated with labels for unpaved roads and well pads. To further enrich the contextual understanding of the dataset, it has been systematically divided into two subsets based on the background landscape. This is discussed in more detail in the methodology section. Nevertheless, the research presented in this paper employed the oil sands mining region in Northern Alberta as its study area, given its varied landscape historical backgrounds and the land disturbances arising from oil and gas exploration activities. A summary and related work on land disturbance mapping and error correction are presented in Section 2. Then, Section 3 focuses on presenting the automatic error-correcting (AEC) algorithm

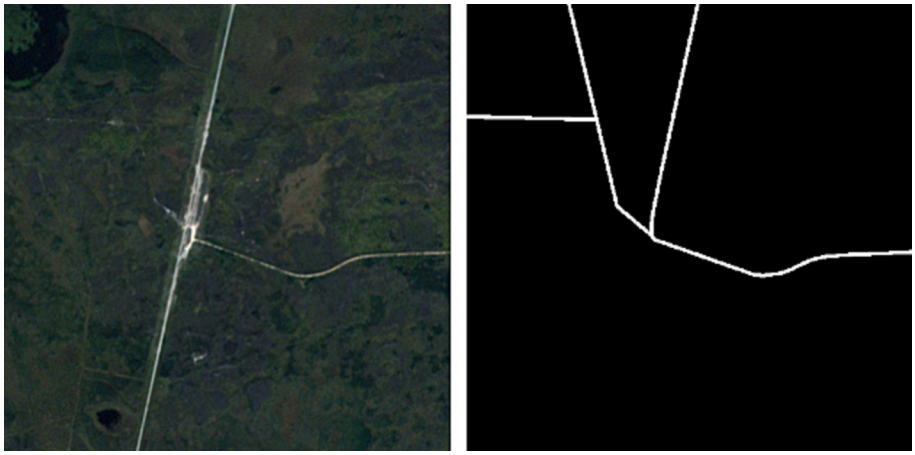

Fig. 1. Examples of image (left) and "ground truth" (right) pair with missing or incorrect labels.

used to enhance model performance by correcting bad examples in the training set during learning. The effectiveness of the AEC algorithm with improved performance when mapping the labelled dataset is explained in Section 4. Following the experiments, results were analyzed, and the capability of the AEC algorithm is further discussed in Section 5. In the final section, the research and the results of the research are summarized.

2. Related works

2.1. Land disturbance mapping

Land disturbances on the Earth's surface exhibit a high degree of diversity and randomness (Senf et al., 2015). Specially, land disturbances related to oil and gas exploitation and exploration has mainly resulted from drill pad construction, common well equipment maintenance, and multiple roads connecting the drill pad (Wang et al., 2020a). The resulting land disturbance related to oil and gas developments can cause environmental damage, including vegetation withering, serious erosion, stream degradation, habitat fragmentation, and even some permanent land cover changes (Doley and Audet, 2013; Wang et al., 2020b). Given its profound significance in environmental management, continuous and relevant research efforts have been dedicated to understanding and mitigating these impacts.

Current land disturbance mapping is divided into two types: spectral trajectory-based detection methods and machine/deep learning-based methods. Spectral trajectory-based detection methods have been commonly used for mapping land disturbances. Recent studies have included the Landsat-based detection of trends in disturbance and recovery (LandTrendr) (Kennedy et al., 2010), continuous change detection and classification (CCDC) (Zhu and Woodcock, 2014), continuous subpixel monitoring (CSM) (Deng and Zhu, 2020), and continuous monitoring of land disturbance (COLD) (Ye et al., 2023). The LT-GEE algorithm (GEE-version Landsat-based detection of trends in disturbance and recovery) was used to detect land disturbances, which mainly referred to the conversion from vegetation to other impervious surfaces (Wang et al., 2020b). LandTrendr could detect the change situation and smooth the entire trend from the image time series stacks (Deng and Zhu, 2020). Although a variety of methods have been applied in land disturbance mapping, efficiency and accuracy can still be further improved.

When focusing on research related to quantifying the impact of surface mining activity and reclamation, except for field surveys, research in the early stage mainly used machine learning algorithms such as random forest (RF), support vector machines (SVMs), and CNN-based networks. The performances with SVMs on land disturbances detection caused by drilling need improvement (Temitope et al., 2020), while CNNs-based models, such as mask-region-based convolutional neural networks (mask R-CNNs), were mainly used in oil spill detection. Specifically, with the combination of ResNet and feature pyramid network (FPN) architecture for feature extraction, the model performed better than conventional machine learning models. However, the impacts of mining on its surrounding area have usually been ignored (Sharifi et al., 2015; Yekeen et al., 2020; Zhang and Gao, 2023).

However, there is still an overwhelming number of shortcomings in previous DL-based methods. For instance, FastICA presents notable advantages in terms of simultaneous processing and efficiency, and it has improved results in PolSAR speckle reduction, particularly when applied to polarimetric channels. However, users should be mindful of its interpretational complexity and potential sensitivity to parameters (Sharifi et al., 2015). The multivariate relevance vector regression (MVRVR), while having high estimation accuracy, solves the underestimation problem (Sharifi et al., 2016). However, there is actually a large number of DL-based methods applied in land disturbance detection. Sharifi (2020) used the relevance vector machine (RVM) and SAR data for flood mapping. Although RVM has high efficiency in classification tasks and is capable of sparsity, which selects only relevant vectors for classification to reduce computational complexity, there have been challenges as the RVM model lacks the interpretability of simpler models. The problem of interpretability was then solved by a multiscale dual-branch residual spectral-spatial network (MDBRSSN), but the MDBRSSN also raised a new problem of model complexity (Sharifi, 2021; Ghaderizadeh et al., 2022; Tariq et al., 2022; Farmonov et al., 2023). In the 3D level, the CNNeGA method demonstrates advantages in terms of reducing data volume, increasing processing speed, and improving accuracy in hyperspectral band selection (Esmaeili et al., 2023). However, the complexity introduced and the potential sensitivity to parameter tuning can bring troubles in application. Based on those previous methods, there should be a shift to some newly-proposed methods. A few studies still use deep learning techniques for mapping land disturbances related to oil exploration. For example, Han et al. (2021) applied deep learning methods to map the well pads, the access roads, and the pipelines in the Athabasca oil sands region of Alberta, Canada. They achieved an overall accuracy of 94.5 % for well pads, 96.1 % for access roads, and 97.6 % for pipelines. Similarly, Alshehhi et al. (2021) leveraged deep learning methodologies to delineate alterations in land cover associated with oilfields within the United Arab Emirates. Their study revealed that the application of deep learning techniques proved highly efficacious in accurately discerning and mapping changes attributed to oil exploration activities. In a study conducted in the Permian Basin of West Texas, USA, Zhou et al. (2021) used deep learning to detect and map well pads and associated infrastructure. They achieved an overall accuracy of 94.5 % for well pads and 94.8 % for associated infrastructure. In addition, several other studies have successfully implemented deep learning for mapping land cover changes related to oil exploration activities on a global scale. For instance, Liu et al. (2021) used deep learning to map oil palm plantations in Southeast Asia, while Wu et al. (2020) used deep learning to map oil and gas infrastructure in the Niger Delta region of Nigeria. Overall, these studies demonstrated the potential of deep learning techniques for accurately mapping land disturbances related to oil exploration activities.

2.2. Error correction in model training

Error correction in model training has been applied in many fields, for instance, medical science (Wang et al., 2020a), weather analysis (Duan et al., 2021) and also many other research areas. In the context of error correction in model training, there are typically two main approaches: manual and machine-assisted. The manual approach involves human annotators reviewing and correcting errors in the training data, a process which can be time consuming and costly, especially when dealing with extremely high volumes of data. In contrast, the machine-assisted approach involves using algorithms or tools to automatically identify and correct errors, which can be faster, more efficient, and less expensive. Moreover, with the machine-assisted approach, error correction can be fully automated. For example, a multiple-round training scheme can be set up to correct the ground truth annotations training-round by training-round during optimization (Girard et al., 2019). In general, machine-assisted curation is not applicable between different deep learning tasks, particularly when dealing with a significant volume of deep learning data (Máttyus et al., 2017; Girard et al., 2019; Hu, 2021).

By employing the improved complete ensemble empirical mode decomposition with adaptive noise (ICEEMDAN) method (Wu and Huang, 2009; Colominas et al., 2014; Santhosh et al., 2018; Yang and Wang, 2018), recurrent neural network (RNN), and autoregressive integrated moving average (ARIMA) model (Liu et al., 2015) with an error correction model, errors appearing during the short-term wind speed prediction training phase can be rectified. Thus, the modified data can be subsequently analyzed. Researchers also compared the error correction models in their studies. They found that prediction accuracy is significantly improved when the error-decomposition correction

method is applied in the training process (Wang et al., 2020b, Duan et al., 2021). Among all these methods, DeepEC is an error correction framework that can be applied to deep neural networks for dose prediction and organ segmentation. It shows that when using a prediction or calibration network, the error correction mechanism enhanced the state-of-the-art networks, greatly improving performance compared to previous studies (Wang et al., 2020b, Wei et al., 2023). In general, the error correction process has a positive impact on model training and final performance.

However, it is imperative to acknowledge the inherent limitations of these methods. For instance, while the ICEEMDAN method excels in signal decomposition, it may introduce artifacts or uncertainties, particularly in complex and dynamic datasets. Similarly, the utilization of recurrent neural networks (RNNs) may be susceptible to challenges related to vanishing or exploding gradients, potentially impacting the model's stability during training. Additionally, the autoregressive integrated moving average (ARIMA) model assumes linearity and stationarity in time series data, which could limit its effectiveness in capturing highly nonlinear wind speed patterns.

An exemplary advancement in error correction is the DeepEC framework, explicitly designed for error correction in deep neural networks applied to dose prediction and organ segmentation (Wang et al., 2020b; Wei et al., 2023). While DeepEC has demonstrated considerable performance improvement when integrated into the prediction or calibration networks, it is prudent to consider potential computational overhead and the need for substantial labelled data for training. In summary, despite the positive impact of error correction processes on model training and final performance, a nuanced understanding of the limitations associated with each method is vital for informed and effective application in diverse scenarios.

3. Materials and methods

3.1. Data and pre-processing

The data used in the research covers the area of the Alberta oil sands mining sites. The dataset contains 600 patches, where each patch consists of 500 × 500 pixels. Generated from RapidEye satellite imagery, the images possess a spatial resolution of 5 m. The RapidEye satellite imagery typically comes in digital raster format (DRF), where each pixel in the image corresponds to a specific geographic location with associated spectral information. The dataset consists of three bands, indicating that the imagery used in this research is in RGB format. The imagery utilized in this research emanates from the cutting-edge RapidEye satellite system. Renowned for its high-resolution capabilities, this satellite provides a detailed perspective of the Alberta oil sands mining sites. The 500 × 500 pixel patches offer a fine-grained view of the terrain, facilitating a nuanced understanding of the features present. Within the dataset, a meticulous categorization has been undertaken, focusing on the presence of unpaved roads and well pads. These critical components of the oil sands' infrastructure are delineated within the images, adding a layer of specificity to the dataset.

In the sampling process, the sampling method we applied to generate data is segmentation sampling. In detail, the sampling method involves dividing the spatial data into smaller, manageable segments (patches) to focus on specific areas of interest (well sites and unpaved roads). Each patch is then annotated based on the presence or absence of the annotated features. This method allows for more granular analysis of the area, especially when dealing with large datasets or when specific features are scattered across the region.

To further enhance the contextual understanding of the dataset, it has been partitioned into two subsets based on the background landscape. A majority, consisting of 400 patches, unfolds against the backdrop of the dense and biodiverse forest ecosystem. The remaining 200 patches showcase the juxtaposition of oil-related activities against the canvas of farmland expanses (Fig. 2). By integrating the spatial intricacies of the Alberta oil sands mining sites with the nuances of background landscapes, this research aims to unravel patterns, assess environmental impact, and contribute valuable insight to the ongoing discourse surrounding resource extraction and land use. In understanding the dataset's historical context and intricacies, we embark on a journey to decipher the Alberta oil sands through the lens of sophisticated satellite technology, laying the groundwork for a comprehensive exploration of this dynamic and consequential region. To normalize the pixel values, Equation (1) was used to result in values ranging between 0 and 1 for all patches.

$$\mathrm{Norm}(p_i, \mathrm{img} = \{p_1, p_2, \ldots, p_i, \ldots, p_n\}) = \frac{p_i}{\max(\mathrm{img})} \quad (1)$$

In the data of this research, each patch includes both resource roads and well-pad labels. Each black and white labelled patch corresponds to a RapidEye 500 × 500-pixel image patch. With the satellite images and the labelled images (Fig. 3), the two subsets of the dataset are partitioned into training and validation sets through 10-fold cross-validation. The patches are numbered in sequential order based on their location. A 10-fold division is implemented to guarantee impartial validation scores during error correction and unbiased final testing scores. 60 out of the total 600 patches are set aside for testing, while the remaining 540 patches are employed for the training process.

3.2. Method

The main method in this paper uses MobileNet as the backbone of the DeepLabv3+ architecture. The features extracted by MobileNet are then

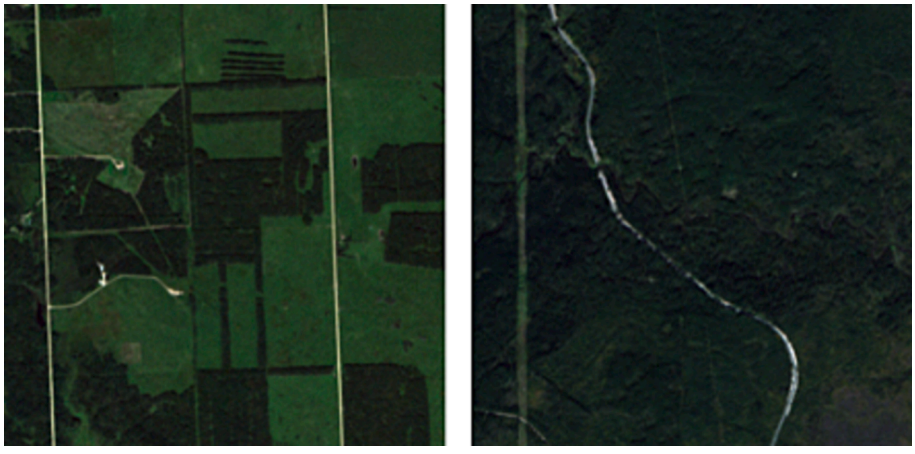

Fig. 2. Images of farmland background (left) and images of forest background (right) in the Alberta oil sands mining sites dataset (Hu, 2021).

Fig. 3. Well-pad label (left), road label (centre), and combined label (right).

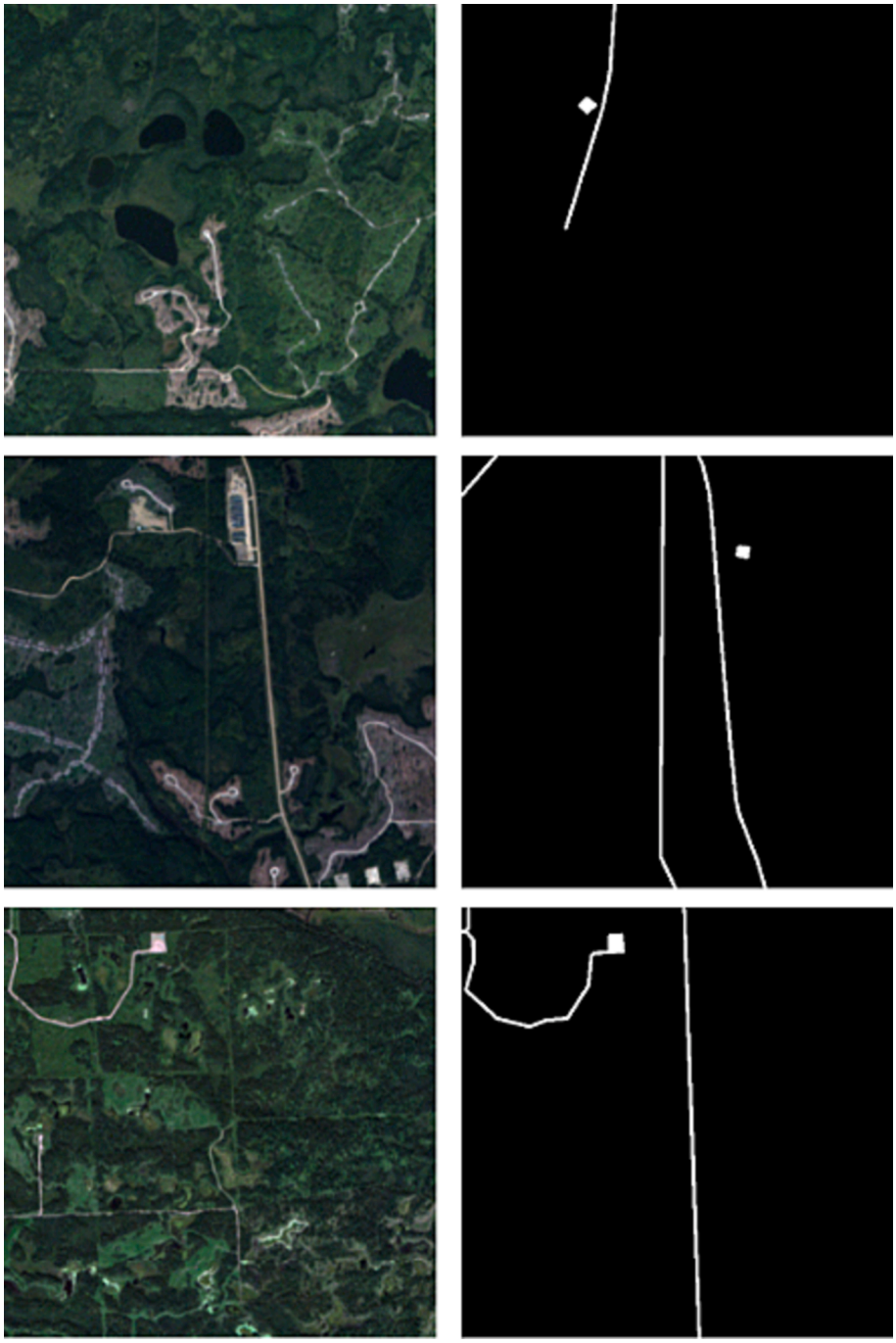

Fig. 4. Errors in the ground truth images (original images [left] and errors [right]).

passed through the DeepLabv3+ module. By combining MobileNet's efficiency with DeepLabv3+'s segmentation capabilities, the method can be suitable for land disturbance detection. The decision to use MobileNet as the model backbone over ResNet was based on its higher efficiency and lower memory cost request, even though it has lower performance than ResNet (Chen et al., 2022). With depth-wise separable convolutions structure and depth multiplier, a few number of parameters and computations are required to preserve the ability to learn useful features from data (Sandler et al., 2018). A compromise of an output stride of 16 was chosen to balance speed and performance. Additionally, the focal loss was utilized to handle potential class imbalance problems in the ground truth labels. Similar to an improved version of the previous DeepLabv3 model, DeepLabv3+, the other parameters are kept as the same as in DeepLabv3+, including a learning rate of 0.01, a polynomial decay schedule, and a momentum of 0.9 (Chen et al., 2018). A training batch size of 32 is chosen to balance speed and performance, with a validation/test batch size of 8. Consistency is maintained by using the same random speed across all experiments. Experiments in this work are executed using Cuda 11.1 on a GeForce RTX 3090 GPU and an AMD Ryzen 9 3900x CPU.

At the core of the AEC algorithm lies the notion of adjusting ground truth corrections based on the model's accuracy degree. The AEC algorithm makes ground truth corrections where it sees fit proportionally to how well the model performs on the validation set. Getting accurate and reliable ground truth labels is not an easy task, and false negative errors commonly appear during the detection process. Even with high-quality datasets like OpenStreetMap and TorontoCity, there exists a 14 % difference in their ground truth labels (Máttyus et al., 2017). The ground truth labels used in this study also have errors, and correcting them can improve the model's performance (Fig. 4).

The key idea of the AEC algorithm lies in the selective updating of pixel probabilities (via hyperparameters α and β) based on the discrepancies between model predictions and ground truths. This update process, governed by the function $f(p^*, V)$, dynamically adjusts the likelihood of pixel updates in the training set, particularly in response to improvements in model accuracy and rising cIoU values on the validation set. The distinctive feature of the AEC algorithm is its innovative approach to dynamically and selectively updating pixel probabilities. This process is guided by hyperparameters α and β, which consider the disparities between model predictions and ground truths. The utilization of these hyperparameters, along with the adaptive updating mechanism facilitated by the functions, presents a unique methodology. This method is designed to respond to advancements in model accuracy and the augmentation of cIoU values within the validation set. Consequently, this contributes significantly to the overall effectiveness of the training process, ensuring improved training outcomes.

Manually correcting mistakes and poor-quality examples is time consuming. However, deep learning frameworks are capable to automatically handle these errors, making manual re-labelling unnecessary. $V = (Y^*, Y)$ represents a validation set with m images, where $Y^* = \{Y_1^*, ..., Y_m^*\}$ denotes the model predictions, and $Y = \{Y_1, ..., Y_m\}$ denotes the corresponding ground truths. Similarly, let $y^* = \{y_1^*, ..., y_n^*\}$ and $y = \{y_1, ..., y_n\}$ represent the model predictions and ground truths, respectively, for a training set with n images. The error correcting probability $P(p|y^*, V)$ can then be calculated as:

$$P(p|y^*, V) = \mathrm{Min}(\mathrm{cIoU}(\mathrm{class}(p^*), V)^{f(p^*,V)}, 1) \tag{2}$$

$$f(p^*, V) = \alpha - \beta^* cIoU(class(p^*), V) \tag{3}$$

where the variables p^* and p represent pixels in one image that correspond to pixels in another image within y and y^*. Hyperparameters α and β play a crucial role in determining the behaviour of the AEC algorithm during training. In Equation (3), $\alpha, \beta > 0, \alpha \neq 0$. The function class() takes a pixel a as input and returns the class label of that pixel, indicating which object or background it belongs to. $\mathrm{cIoU}(c, V)$ is a function that returns the validation set of the intersection over union (IoU) of the predicted class c with the ground truth class c in the validation dataset V. By comparing the pixels of model predictions and ground truths, the structure uses the class() function and cIoU to update the probability. The AEC algorithm can selectively update pixels in y based on the differences between y* and y, in proportion to the respective cIoU values from the validation set and the function $f(p^*, V)$. The probability $P(p|y^*, V)$ represents the likelihood of the error-correcting (EC) probability for pixel p in y by updating it to match the corresponding pixel p^* in y^* based on the validation dataset V. When the model's accuracy improves and cIoU values rise in the validation set, the likelihood of making updates in the training set also increases (Fig. 4).

Fig. 5 depicts the workflow of the AEC algorithm. The model's validation performance was subsequently used to calculate the probability of error correction. In detail, the AEC algorithm is executed alongside validation testing at regular intervals during model training. It does not modify the validation set, ensuring its independence throughout the training process. Since the validation set remains unchanged, any performance enhancements observed in the validation set during AEC algorithm execution are solely attributed to the algorithm itself. The outline of the proposed algorithm is as follows:

Algorithm 1. *Outline of Pseudocode for the AEC Algorithm.*

```
for image im*i in y* do
for pixel p* in im*i do
c ← class(p*)
cIoU ← cIoU (c, V)
probability ← Min(cIoU^α, 1)
if Random(probability) == True then
p → p*
end if
end for
end for
```

3.3. Evaluation

In this research, the evaluation metrics selected are average pixel accuracy (AA) and intersection over union (IoU). AA represents the accuracy of segmentation in terms of pixels, on average, compared to the ground truth labels. AA is given by

$$AA = \mathrm{Avg}(\mathrm{pixelAccuracy}(img_1), ..., \mathrm{pixelAccuracy}(img_n)) \tag{4}$$

where n denotes the sum number of images, $\mathrm{pixelAccuracy}(img_i)$ calculates the accuracy at pixel-level for the i^{th} image, and the function "Avg(…)" calculates the mean value of a set of numbers.

Intersection over union (IoU) is a useful evaluation metric applied to computer vision and object detection tasks. It is also used in the evaluation process of the proposed method (Rahman and Wang, 2016). IoU is given by

$$\mathrm{IoU} = \frac{|Y^* \cap Y|}{|Y^* \cup Y|} \tag{5}$$

To evaluate the accuracy of segmentation models, the intersection over union (IoU) metric is used, which compares the predicted segmentation (Y^*) to the ground truth (Y) for each class (cIoU). The mean intersection over union (mIoU) is determined by averaging the class intersection over union (cIoUs), thus treating segmentation inaccuracies uniformly across all classes despite their ground truth frequency (Rahman and Wang, 2016). Both cIoUs and mIoU are effective in evaluating the proposed AEC algorithm, as they measure the accuracy of segmentation models and are unbiased despite class imbalance.

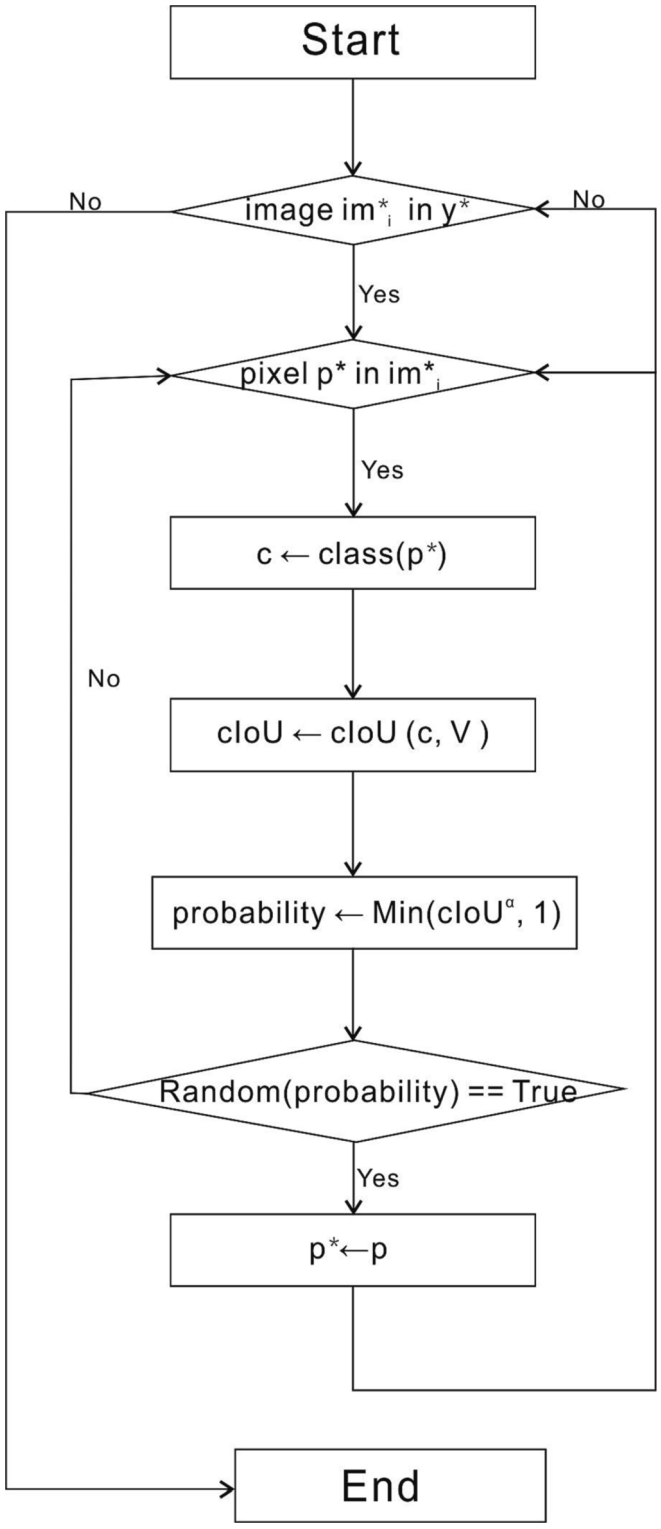

Fig. 5. Workflow of the AEC algorithm.

4. Experimental analysis and results

4.1. Experiments

Five comparative experiments were conducted. Baseline experiments (Experiments 1 and 2) were conducted without the AEC algorithm experiments, and the AEC algorithm was then applied to Experiments 3, 4, and 5) (Table 1). First, baseline Experiments 1 and 2 were conducted without the AEC algorithm. Then, Experiments 3 and 4 were trained for 10 k iterations, and the AEC algorithm was applied to both the forest and the farmland background images with every 200 training iterations. Subsequently, the AEC algorithm was run in every training iteration until the model achieved the best mIoU score in Experiment 5. Here, hyperparameter α is a parameter that determines error correction probability given cIoU (Fig. 6). The values of α were selected arbitrarily in order to showcase the performance of the AEC algorithm across a range of conditions, and they can be further refined through optimization to enhance the overall efficacy of the model. When the value of α changed, the error correction probability also changed. If encountering the same class IoU, the increased value of α can lead to enhancing error correction probability limitations. The error correction probability can undergo a great increase when class IoU reaches a relatively high value with an increased value of α (Fig. 6). Therefore, the experiments for the AEC algorithm involved its performance testing while modifying the image background and adjusting the value of α.

Table 1
Experimental settings and results for the baseline experiments and AEC algorithm-added experiments.

#	Background	α	Interval	AA (%)	mIoU (%)
1	Forest	–	–	58.8	56.4
2	Farmland	–	–	76.7	70.2
3	Forest	2	200	67.9	59.7
4	Farmland	5	200	83.1	70.6
5	Farmland	5	On Best	84.6	70.5

4.2. Results and discussion

In the evaluation process of the algorithm, two key metrics that are commonly used in evaluating the performances of DL-based methods on change detection, average pixel accuracy (AA) and mean intersection over union (mIoU), were employed. These metrics were selected due to their ability to comprehensively assess the accuracy and spatial overlap of land disturbance extraction results, providing insights into the model's effectiveness across diverse backgrounds.

When not applying the AEC algorithm to the experiments, the baseline results show that the AA and mIoU reach 58.8 % and 56.4 % in the forest background while achieving higher values in the farmland background, which reaches 76.7 % and 70.2 %, respectively (Experiments 1 and 2). The results show the best model performance after 30 k training iterations. While applying the AEC algorithm to Experiments 3 and 4, both AA and mIoU reached higher values. In detail, the AA and mIoU reach 67.9 % and 59.7 % in the forest background while achieving higher values in the farmland background, which reaches 83.7 % and 70.6 %, respectively. Especially when trying to run every training iteration until the model achieved the best mIoU score, as in Experiment 5, the AA can reach an even higher score of 84.6 %. The results show that applying the AEC algorithm to the model leads to great effectiveness (Table 1).

For Experiments 1 and 3, significant performance improvements can be observed with the AEC algorithm in comparison to the baseline control ones (Fig. 7). In detail, the experiment of land disturbance extraction from forest areas utilizing the AEC algorithm demonstrated notable enhancements in both the average pixel accuracy (AA) and mean intersection over union (mIoU) scores, which achieved a respective increase of 15.4 % and 5.8 % over the baseline.

Similarly, when comparing Experiment 2 and Experiment 4, the AEC algorithm was shown to enhance the performances of land disturbance extraction in farmland, resulting in a respective increase of 8.3 % and 0.5 % in AA and mIoU scores. Therefore, the efficiency of the AEC algorithm in updating labels for farmland and forest imagery is prominent (Fig. 8).

Specifically, AA shows an increase of 9.1 %, and mIoU shows an

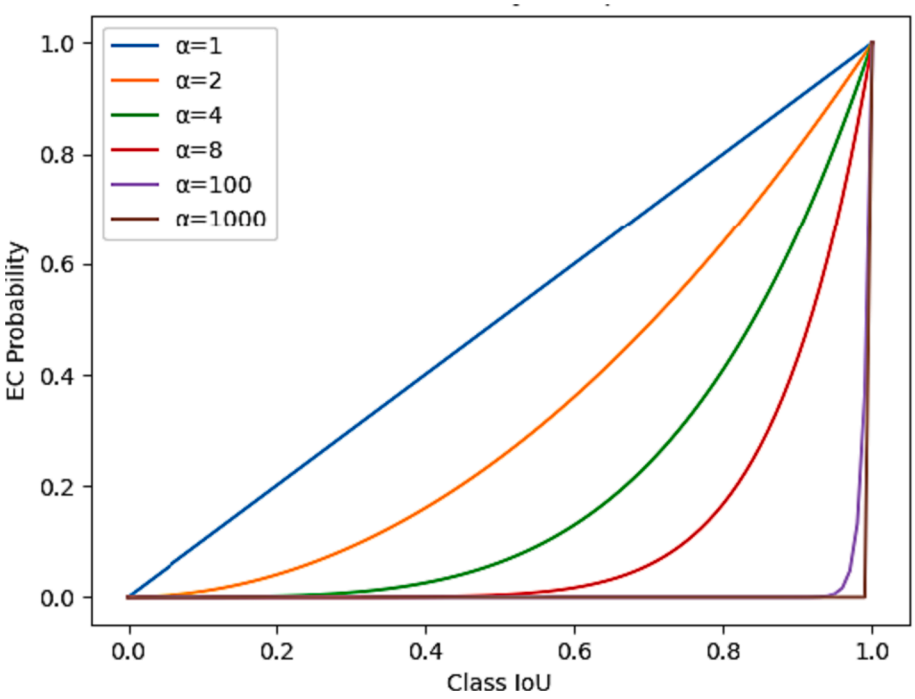

Fig. 6. Relationship between α value changes and the slope of the EC probability curve.

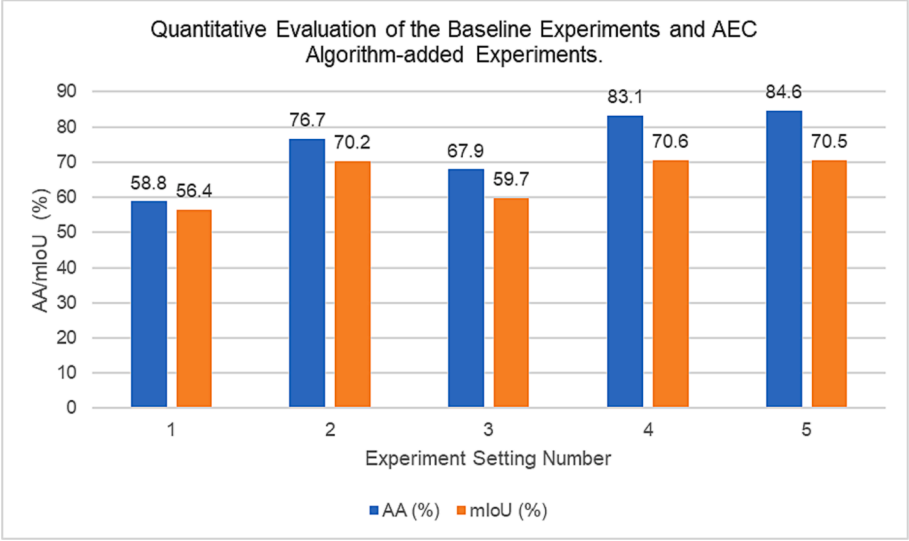

Fig. 7. Bar chart of quantitative evaluation on the baseline experiments and AEC algorithm-added experiments (experiment number settings refer to Table 1).

increase of 3.3 % with the forest background, which is much higher than the 7.0 % increase in AA and 0.4 % increase in mIoU with the farmland background. These percentages indicate that, although the oil-related land disturbance detection is more accurate with the farmland background, the elevation on the performance is greater when experimenting with the AEC algorithm on the forest background (Table 1).

Besides, both AA and mIoU can exhibit a much steeper increase with respect to training iterations when using AEC as opposed to the baseline (Fig. 9 and Fig. 10). This can be explained further as the AEC training process involves both dataset improvement and model fitting. However, this difference in behavior was not observed in the initial 1000 iterations. This is potentially due to the learning rate schedule along with the AEC requiring warm-up since the model does not understand what a correct prediction is and what needs to be corrected at the start of the training. To further evaluate the practical application of the AEC algorithm, we conducted additional analysis by comparing Experiments 3 and 4 with Experiment 5. The results indicate that the "On Best" experiment needs fewer updates than the other experiments but can attain comparable performance (Table 1).

Experiment 5 made a total of 18 updates compared to the 50 made in Experiments 3 and 4. The experimental results indicate that Experiment 5, which involves only 36 % of the updates made in Experiments 3 and 4, achieved a similar performance. This observation suggests that the AEC algorithm can enhance the performance with a minimal set of strategically selected updates. However, although the AEC algorithm helps enhance the ground truth data quality, space remains for more improvements. The correction probability can also be improved in future studies by testing different evaluation metrics, especially statistical ones. More deep neural architectures should also be tested in conjunction with AEC to ascertain its dependence on neural architecture and

Fig. 8. Examples of error correction results: forest (left) and farmland (right), original ground truth (top), image (middle), and AEC updated ground truth (bottom).

achieve better overall performance.

By applying state-of-the-art deep learning methods and AEC to detect oil-exploration-related land disturbances, these methods can prevent ignorance of land encroachment and destruction during and after hydrocarbon development. The results demonstrate that the AEC algorithm can substantially enhance the precision of land disturbance detection from satellite images employing deep learning techniques. The practical implications of the AEC algorithm are wide-ranging, with potential benefits in the fields of land management, agriculture, and forestry. The adoption of AEC can greatly enhance the applicability and deployment of deep learning models for precise land management and planning by improving the quality of both models and datasets. Moreover, the AEC algorithm is particularly useful in scenarios where the images are up to date, but the corresponding labels are not.

However, while the AEC algorithm has demonstrated effectiveness in the Alberta dataset, further experiments are slated to assess its performance on datasets exhibiting similar scattered land disturbance patterns. Additionally, despite notable enhancements in ground truth data quality by applying the AEC algorithm, there remains room for refinement. Even after implementing the AEC algorithm into the network, the average accuracy for detecting land disturbances in forested areas only reached 67.9 %. This level of accuracy may not suffice for rigorous land disturbance analysis, potentially impacting critical government planning decisions. Therefore, ongoing efforts to enhance the algorithm's performance are imperative for robust and reliable land protection planning.

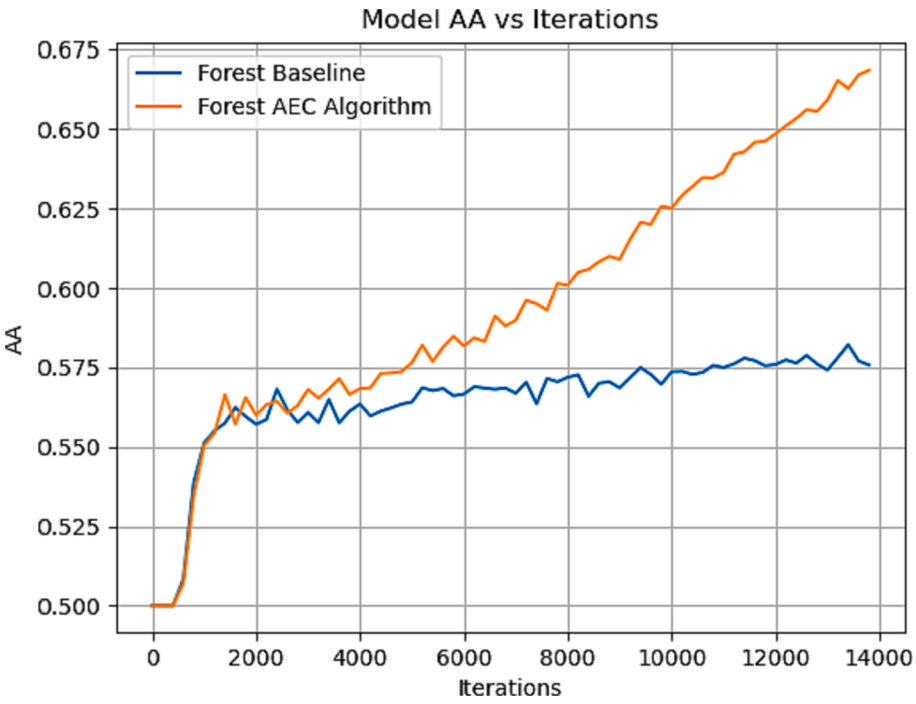

Fig. 9. Comparison of average pixel accuracy (AA) vs iterations between forest control and baseline AEC algorithm.

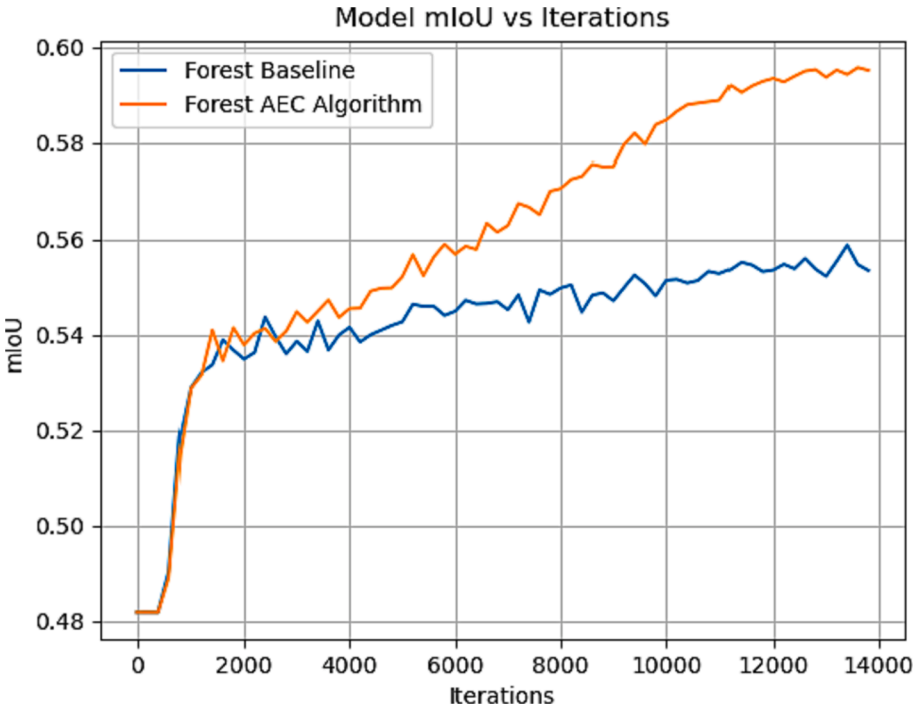

Fig. 10. Comparison of mIoU performance between forest control and AEC baseline over iterations.

5. Discussion

The AEC algorithm exhibits commendable performance in error correction, offering promising prospects for advancing the mapping of future land disturbances. However, it is imperative to delve into its computational cost for a comprehensive evaluation. Compared with other existing methods, during the training phase, AEC's forward pass aligns with the neural network's architecture, while its integration in the backward pass introduces additional complexity, impacting gradient computation and parameter updates. The error correction process, involving error identification and label updating, is linear but contributes to the overall complexity. During deployment, AEC's computational complexity is determined by the neural network architecture and input size. Compared to traditional manual or heuristic correction, AEC provides an automated alternative, proving advantageous for efficiency and adaptability in model learning dynamics. Although AEC demonstrates a manageable computational load and the potential to enhance model accuracy, particularly in datasets prone to labeling errors, it may possess

a lower computational overhead than some advanced error correction techniques. In general, the AEC algorithm outperformed other existing methods, such as ICEEMDAN network (Wu and Huang, 2009; Colominas et al., 2014; Santhosh et al., 2018; Yang and Wang, 2018), RNN, and ARIMA model (Liu et al., 2015). Its superiority positions it as a valuable tool for error correction in deep learning models, particularly in scenarios where datasets are susceptible to labeling errors. While acknowledging its merits, ongoing research and fine-tuning are recommended to optimize AEC's performance for specific applications and architectures, ensuring its continued effectiveness and adaptability.

Despite the advancements demonstrated by our proposed automatic error-correcting (AEC) algorithm, there are noteworthy limitations that should be acknowledged. While our study demonstrates notable performance elevation with the automatic error-correcting (AEC) algorithm in the context of farmland background, the extent of improvement is comparatively modest in scenarios involving the forest background. This discrepancy could potentially translate into variations in land disturbance mapping accuracy. This constitutes the initial limitation of our proposed method. Additionally, it is important to acknowledge that our current investigation has solely focused on farmland and forest backgrounds, neglecting the broader spectrum of areas where oil exploration activities may occur. Oil exploration is not confined to terrestrial landscapes but extends to marine environments and urban areas. Given the limited dataset employed in our research, the efficacy of the AEC algorithm in mapping land disturbances in these diverse contexts, such as sea areas and urban environments, remains unexplored. As a result, the generalizability and performance of our AEC algorithm in mapping land disturbances in these specific regions warrant further investigation and testing.

6. Conclusion

In this paper, we propose an automatic error-correcting algorithm (AEC) tailored to the context of Alberta oil sands, specifically designed to rectify errors in road and well-pad extraction during training to address the common inherent imperfections in deep-learning data. Comparative analyses between the baseline and AEC-enhanced models demonstrate a substantial improvement in the performance of detecting land disturbances associated with oil exploration. Our findings reveal that the proposed algorithm contributes to an enhancement of 8.3 % to 15.4 % in average accuracy (AA) and a 0.5 % to 5.8 % improvement in mean intersection over union (mIoU). Significantly, while oil-related land disturbance detection accuracy is notably higher in the farmland background, the AEC algorithm exhibits a more pronounced performance elevation when applied to the forest background. In summary, our AEC algorithm demonstrates its efficacy in automatically and efficiently rectifying data errors during land disturbance detection. This positions it as a valuable tool for mapping unpaved rural roads and objects, thereby significantly improving dataset quality and enhancing the performance of intelligent training models for mapping disturbances related to oil exploration.

Declaration of competing interest

The authors declare that they have no known competing financial interests or personal relationships that could have appeared to influence the work reported in this paper.

References

Abdelfatah, M.A., 2023. Improving the performance of tropospheric mapping function in low elevation angle using artificial neural network. Egypt. J. Remote Sens. Space Sci. 26 (1), 129–139. https://doi.org/10.1016/j.ejrs.2022.12.011.

Alshehhi, R., Alsuwaidi, A., Almazroui, A., Mahmood, T., 2021. Mapping oilfield related land cover changes in the United Arab Emirates using deep learning. J. Appl. Remote Sens. 15 (2), 024512.

Chen, L., Ding, Y., Pirasteh, S., Hu, H., Zhu, Q., Ge, X., Zeng, H., Yu, H., Shang, Q., Song, Y., 2022. Meta-learning an intermediate representation for few-shot block-wise prediction of landslide susceptibility. Int. J. Appl. Earth Obs. Geoinf. 110, 102807 https://doi.org/10.1016/j.jag.2022.102807.

Chen, W., Zhou, G., Liu, Z., Li, X., Zheng, X., Wang, L., 2022. NIGAN: A framework for mountain road extraction integrating remote sensing road-scene neighborhood probability enhancements and improved conditional generative adversarial network. IEEE Trans. Geosci. Remote Sens. 60, 1–15.

Chen, L.C., Zhu, Y., Papandreou, G., Schroff, F., Adam, H., 2018. Encoder-decoder with atrous separable convolution for semantic image segmentation. Proc. Eur. Conf. Comput. Vis. (ECCV) 801–818.

Chowdhury, S., Peddle, D.R., Wulder, M.A., Heckbert, S., Shipman, T.C., Chao, D.K., 2021. Estimation of land-use/land-cover changes associated with energy footprints and other disturbance agents in the Upper Peace Region of Alberta Canada. Int. J. Appl. Earth Obs. and Geoinf. 94, 102224 from 1985 to 2015 using Landsat data.

Colominas, M.A., Schlotthauer, G., Torres, M.E., 2014. Improved complete ensemble EMD: A suitable tool for biomedical signal processing. Biomed Signal Process Control. 14, 19–29.

Deng, C., Zhu, Z., 2020. Continuous subpixel monitoring of urban impervious surface using Landsat time series. Remote Sens. Environ 238, 110929.

Dimitrovski, I., Kitanovski, I., Kocev, D., Simidjievski, N., 2023. Current trends in deep learning for Earth observation: An open-source benchmark arena for image classification. ISPRS J. Photogramm. Remote Sens. 197, 18–35. https://doi.org/10.1016/j.isprsjprs.2023.01.014.

Doley, D., Audet, P., 2013. Adopting novel ecosystems as suitable rehabilitation alternatives for former mine sites. Ecol. Process. 2, 1–11.

Duan, J., Zuo, H., Bai, Y., Duan, J., Chang, M., Chen, B., 2021. Short-term wind speed forecasting using recurrent neural networks with error correction. Energy 217, 119397.

Esmaeili, M., Abbasi-Moghadam, D., Sharifi, A., Tariq, A., Li, Q., 2023. Hyperspectral image band selection based on CNN embedded GA (CNNeGA). IEEE J. Selected Top. Appl. Earth Obs. Remote Sens. 16, 1927–1950.

Farmonov, N., Amankulova, K., Szatmári, J., Sharifi, A., Abbasi-Moghadam, D., Nejad, S. M.M., Mucsi, L., 2023. Crop type classification by DESIS hyperspectral imagery and machine learning algorithms. IEEE J. Select Top. Appl. Earth Obs. Remote Sens. 16, 1576–1588.

Fu, L., Chen, X., Pirasteh, S., Xu, Y., 2023. Classification of hyperspectral images: Double-branch multi-scale residual network. Remote Sens. 15 (18), 4471. https://doi.org/10.3390/rs15184471.

Ghaderizadeh, S., Abbasi-Moghadam, D., Sharifi, A., Tariq, A., Qin, S., 2022. Multiscale dual-branch residual spectral-spatial network with attention for hyperspectral image classification. IEEE J. Select Top. Appl. Earth Obs. Remote Sens. 15, 5455–5467.

Girard, N., Charpiat, G., and Tarabalka, Y., 2019. Noisy supervision for correcting misaligned cadaster maps without perfect ground truth data. *In IGARSS 2019-2019 IEEE Int. Geosci. Remote Sens. Symp.*, July 2019, pp. 10103–10106. IEEE.

Habibi, A., Delavar, M.R., Sadeghian, M.S., Nazari, B., Pirasteh, S., Li, J., 2023. A hybrid of ensemble machine learning models with RFE and Boruta Wrapper-based algorithms for flash flood susceptibility assessment. Int. J. Appl. Earth Obs. Geoinf. 122, 103401 https://doi.org/10.1016/j.jag.2023.103401.

Han, Z., Li, X., Zhang, S., Ma, Y., Liu, X., 2021. Mapping well pads, access roads, and pipelines in the Athabasca oil sands region with deep learning. ISPRS J. Photogramm. Remote Sens. 174, 16–28.

He, K., Zhang, X., Ren, S., and Sun, J., 2016. Deep residual learning for image recognition. *In Proc. IEEE Conf. Comput. Vis. Patt. Recog.*, Las Vegas, NV, USA, 27–30 June, pp. 770–778.

Hu, B. (2021). Land Disturbance Extraction in Alberta Oil Sands Satellite Imagery. UWSpace. http://hdl.handle.net/10012/17750.

Jordaan, S., Keith, D., Stelfox, B., 2009. Quantifying land use of oil sands production: A life cycle perspective. Environ. Res. Lett. 4 (2), 024004 https://doi.org/10.1088/1748-9326/4/2/024004.

Kearney, S.P., Coops, N.C., Sethi, S., Stenhouse, G.B., 2020. Maintaining accurate, current, rural road network data: An extraction and updating routine using RapidEye, participatory GIS and deep learning. Int. J. Appl. Earth Obs. Geoinf. 87, 102031 https://doi.org/10.1016/j.jag.2019.102031.

Kennedy, R.E., Yang, Z., Cohen, W.B., 2010. Detecting trends in forest disturbance and recovery using yearly Landsat time series: 1. LandTrendr—Temporal segmentation algorithms. Remote Sens. Environ. 114 (12), 2897–2910.

Khorrami, B., Pirasteh, S., Ali, S., Sahin, O.G., Vaheddoost, B., 2023. Statistical downscaling of GRACE TWSA estimates to a 1-km spatial resolution for a local-scale surveillance of flooding potential. J. Hydrol., 129929 https://doi.org/10.1016/j.jhydrol.2023.129929.

Kosari, A., Sharifi, A., Ahmadi, A., Khoshsima, M., 2020. Remote sensing satellite's attitude control system: Rapid performance sizing for passive scan imaging mode. Aircraft Eng. Aeros. Techn. 92 (7), 1073–1083.

Laurence, W.F., Balmford, A., 2013. A global map for road building. Nature 495 (7441), 308–309. https://doi.org/10.1038/495308a.

Li, Y., Huang, W., Lyu, X., Liu, S., Zhao, Z., Ren, P., 2022. An adversarial learning approach to forecasted wind field correction with an application to oil spill drift prediction. Int. J. Appl. Earth Obs. Geoinf. 112, 102924.

Li, W., Zhu, J., Pirasteh, S., Zhu, Q., Fu, L., Wu, J., 2022. Investigations of disaster information representation from geospatial perspective: Progress, challenges, and recommendations. Trans. GIS. https://doi.org/10.1111/tgis.12922, 00:1-23.

Liu, H., Tian, H.Q.Q., Li, Y.F.F., 2015. An EMD-recursive ARIMA method to predict wind speed for railway strong wind warning system. J. Wind. Eng. Ind. Aerodyn. 141, 27–38.

Liu, H., Wang, Y., Pang, S., Wang, X., He, J., Zhang, J., Rodriguez-Dono, A., 2022. Mining footprint of the underground longwall caving extraction method: A case study of a typical industrial coal area in China. J. Hazard. Mater. 425, 127762.
Liu, W., Xiao, X., Feng, X., Chen, B., Yang, X., Zhu, L., 2021. Mapping oil palm plantations using dense optical and SAR time series imagery and deep learning in Southeast Asia. Remote Sens. 13 (4), 646.
Ma, L., Li, Y., Li, J., Junior, J.M., Gonçalves, W.N., Chapman, M.A., 2021. Boundarynet: Extraction and completion of road boundaries with deep learning using mobile laser scanning point clouds and satellite imagery. IEEE Trans. Intell. Transp. Syst. 23 (6), 5638–5654.
Maggiori, E., Tarabalka, Y., Charpiat, G., Alliez, P., 2016. Convolutional neural networks for large-scale remote-sensing image classification. IEEE Trans. Geosci. Remote Sens. 55, 645–657.
Máttyus, G., Luo, W., Urtasun, R., 2017. Deep road mapper: Extracting road topology from aerial images. *Proc. IEEE Int. Conf. Comput. Vis.* 3438–3446.
Rahman, M., Wang, Y., 2016. Optimizing intersection-over-union in deep neural networks for image segmentation. Int. Symp. Visual Comput. 234–244. https://doi.org/10.1007/978-3-319-50835-1_22.
Rokosh, C., Lyster, S., Anderson, S., Beaton, A., Berhane, H., Brazzoni, T., Chen, D., Cheng, Y., Mack, T., Pana, C., and Pawlowicz, J., 2012. Summary of Alberta's shale- and siltstone-hosted hydrocarbon resource potential. *Energy Resources Conservation Board*, ERCB/AGS Open File Report, 6, pp. 327.
Safari, O.H., Pirasteh, S., Mansour, S., 2011. Role of Kazerun fault for localizing oil seepage in Zagros mountain Iran: An application of GiT. Remote Sens. 32 (1), 1–16.
Sandler, M., Howard, A., Zhu, M., Zhmoginov, A., & Chen, L. C., 2018. Mobilenetv2: Inverted residuals and linear bottlenecks. *In Proc. IEEE Conf. Comput. Vis. Patt. Recog.*, pp. 4510–4520.
Santhosh, M., Venkaiah, C., Kumar, D.V., 2018. Ensemble empirical mode decomposition based adaptive wavelet neural network method for wind speed prediction. Energy Convers. Manag. 168, 482–493.
Senf, C., Pflugmacher, D., Wulder, M.A., Hostert, P., 2015. Characterizing spectral-temporal patterns of defoliator and bark beetle disturbances using Landsat time series. Remote Sens. Environ. 170, 166–177.
Ševo, I., Avramović, A., 2016. Convolutional neural network based automatic object detection on aerial images. IEEE Geosci. Remote Sens. Lett. 13 (5), 740–744.
Shao, Z., Zhou, Z., Huang, X., Zhang, Y., 2021. MRENet: Simultaneous extraction of road surface and road centerline in complex urban scenes from very high-resolution images. Remote Sens. 13 (2), 239. https://doi.org/10.3390/rs13020239.
Sharifi, A., 2020. Flood mapping using relevance vector machine and SAR data: A case study from Aqqala, Iran. J. Indian Soc. Remote Sens. 48 (9), 1289–1296.
Sharifi, A., 2021. Development of a method for flood detection based on Sentinel-1 images and classifier algorithms. Water Environ. J. 35 (3), 924–929.
Sharifi, A., Amini, J., Sri Sumantyo, J.T., Tateishi, R., 2015. Speckle reduction of PolSAR images in forest regions using fast ICA algorithm. J. Indian Society Remote Sens. 43, 339–346.
Sharifi, A., Amini, J., 2015. Forest biomass estimation using synthetic aperture radar polarimetric features. J. Appl. Remote Sens. 9 (1), 097695 https://doi.org/10.1117/1.JRS.9.097695.
Sharifi, A., Amini, J., Tateishi, R., 2016. Estimation of forest biomass using multivariate relevance vector regression. Photogram. Eng. Remote Sens. 82 (1), 41–49.
Simonyan, K., and Zisserman, A., 2014. Very deep convolutional networks for large-scale image recognition. arXiv2014, arXiv:1409.1556.
Sun, L., Tang, Y., Zhang, L., 2017. Rural building detection in high-resolution imagery based on a two-stage CNN model. IEEE Geosci. Remote Sens. Lett. 14 (11), 199–2002.
Tariq, A., Yan, J., Ghaffar, B., Qin, S., Mousa, B.G., Sharifi, A., Aslam, M., 2022. Flash flood susceptibility assessment and zonation by integrating analytic hierarchy process and frequency ratio model with diverse spatial data. Water 14 (19), 3069.
Temitope, Y.S., Balogun, A., Wan Yusof, K.B.B., 2020. A novel deep learning instance segmentation model for automated marine oil spill detection. ISPRS J. Photogramm. Remote Sens. 167, 190–200. https://doi.org/10.1016/j.isprsjprs.2020.07.01.
Thiessen, R.J., Achari, G., 2022. Predicting negative community responses to upstream oil and gas activities using Alberta's abandoned well sites as an example. Can. J. Civ. Eng. 49 (12), 1807–1818.
Volpi, M., Tuia, D., 2017. Dense semantic labeling of subdecimeter resolution images with convolutional neural networks. IEEE Trans. Geosci. Remote Sens. 55 (2), 881–893.
Wang, Z., Lechner, A.M., Yang, Y., Baumgartl, T., Wu, J., 2020b. Mapping the cumulative impacts of long-term mining disturbance and progressive rehabilitation on ecosystem services. Sci. Total Environ. 717, 137–214.
Wang, H., Zhang, H., Hu, J., Song, Y., Bai, S., Yi, Z., 2020a. DeepEC: An error correction framework for dose prediction and organ segmentation using deep neural networks. Int. J. Intell. Syst. 35 (12), 1987–2008.
Wei, Y., Chen, Z., Zhao, C., Chen, X., He, J., Zhang, C., 2023. A three-stage multi-objective heterogeneous integrated model with decomposition-reconstruction mechanism and adaptive segmentation error correction method for ship motion multi-step prediction. Adv. Eng. Inform. 56, 101954.
Wu, Z., Huang, N.E., 2009. Ensemble empirical mode decomposition: A noise-assisted data analysis method. Adv. Adapt Data Analysis 1 (01), 1–41.
Wu, Y., Xu, B., Jiang, Y., Guo, Y., Wang, J., 2020. Deep learning for oil and gas infrastructure detection in the Niger Delta region using Sentinel-2 imagery. Remote Sens. 12 (12), 1948.
Yang, Z., Li, J., Zipper, C.E., Shen, Y., Miao, H., Donovan, P.F., 2018. Identification of the disturbance and trajectory types in mining areas using multitemporal remote sensing images. Sci. Total Environ. 644, 916–927.
Yang, Z., Wang, J., 2018. A hybrid forecasting approach applied in wind speed forecasting based on a data processing strategy and an optimized artificial intelligence algorithm. Energy 160, 87–100.
Ye, S., Zhu, Z., Cao, G., 2023. Object-based continuous monitoring of land disturbances from dense Landsat time series. Remote Sens. Environ. 287, 113462.
Yeh, C., Perez, A., Driscoll, A., Azzari, G., Tang, Z., Lobell, D., Ermon, S., Burke, M., 2020. Using publicly available satellite imagery and deep learning to understand economic well-being in Africa. Nat. Comm. 11 (1), 2583. https://doi.org/10.1038/s41467-020-16185-w.
Yekeen, S.T., Balogun, A.-L., Khamaruzaman, B., Yusof, W., 2020. A novel deep learning instance segmentation model for automated marine oil spill detection. ISPRS J. Photogramm. Remote Sens. 167, 190–200. https://doi.org/10.1016/j.isprsjprs.2020.07.011.
Zhang, F., Gao, Y., 2023. Composite extraction index to enhance impervious surface information in remotely sensed imagery. Egypt. J. Remote Sens. Space Sci. 26 (1), 141–150. https://doi.org/10.1016/j.ejrs.2022.12.013.
Zhang, Y., Lantz, N., Guindon, B., Jiao, X., 2017. Spectral-analysis-based extraction of land disturbances arising from oil and gas development in diverse landscapes. J. Appl. Remote Sens. 11 (1), 015026. https://doi.org/10.1117/1. JRS.11.015026.
Zhou, Y., Zhang, S., Zhang, C., 2021. Automatic detection and mapping of well pads and related infrastructure using deep learning in the Permian Basin of West Texas. Remote Sens. 13 (13), 2529.
Zhu, Z., Woodcock, C.E., 2014. Continuous change detection and classification of land cover using all available Landsat data. Remote Sens. Environ. 144, 152–171.